Soft Computing (2023) 27:3751–3763
https://doi.org/10.1007/s00500-022-07511-z

OPTIMIZATION

Designing of neural network-based SoSMC for autonomous underwater vehicle: integrating hybrid optimization approach

Rupam Gupta Roy[1] · Girish Vithalrao Lakhekar[2] · Muhammad Hassan Tanveer[3]

Accepted: 7 September 2022 / Published online: 23 November 2022

Abstract
The control of an autonomous underwater vehicle (AUV) is regarded as a difficult challenge, owing to the nonlinear and uncertain dynamics of the AUV. In this work, Optimized neural network (NN) is integrated with the "second-order sliding mode control (SoSMC) approach" for control of yaw angle in AUV. More particularly, the positive gain of SoSMC is predicted by an optimized NN model, where the training is performed by a novel Sea Lion Distance-based FireFly algorithm via tuning the optimal weights. At last, the supremacy of the adopted model is validated under various measures. Accordingly, the RMSE values accomplished by the proposed model is 40.94%, 1.39%, 0.69%, 0.69% and 0.41% better than existing models like "GW-SMC, FF-SoSMC, SLnO-SoSMC, POA-SoSMC and GW-SoSMC", respectively, for set point 1.

Keywords Underwater vehicles · SMC · Neural network · FireFly algorithm · SLD-FA algorithm

Abbreviations

AUV	Autonomous underwater vehicle
CB	Center of buoyancy
EKF	Extended Kalman filter
FoSMC	First-order SMC
FF	Firefly algorithm
FC	Fuzzy controller
GSTA	Generalized super-twisting algorithm
LQR	Linear quadratic regulator
LMI	Linear matrix inequality
NN	Neural network
PID	Proportional integral derivative
RBF-NN	Radial basis function neural network
SMC	Sliding mode controller
SoSMC	Second-order sliding mode controller
SLnO	Sea lion optimization
TDE	Time delay estimation
UML	Unified modelling language

✉ Rupam Gupta Roy
royrupamgupta@gmail.com

1 Department of Electronics and Instrumentation Engineering, National Institute of Technology, Agartala, Barjala, Jirania, Agartala, Tripura, India

2 Department of Instrumentation Engineering, College of Engineering, Pune, Maharashtra, India

3 Department of Robotics and Mechatronics Engineering, Kennesaw State University, Marietta, GA 30067, United States

1 Introduction

Autonomous underwater vehicles (AUVs) have become increasingly important in a variety of underwater missions, including military applications, salvage operations, as well as fisheries research. "AUVs are robotic devices which travel underwater to perform a set of predefined tasks such as accurate navigation, control and guidance tasks without operator intervention" (Woods et al. 2012; Cui et al. 2016; Li and Su 2016). Initially, the AUV was developed by researchers from the University of Washington as early as 1957, which stimulated several other researchers to analyse in this field. Numerous methods have been introduced for controlling the motion of AUV (Petrich and Stilwell 2011; Li et al. 2015a, b). The AUV is much helpful to be deployed in hazardous operations. The safer way to travel around the underwater is by utilizing small unmanned vehicles to perform diverse measurements and missions without risking the lives of people (Shaik et al. 2016; Mastan Sharif et al. 2018) (Sinjari et al. 2019; Qianwen 2021) (Mahdi et al. 2021). With the initiation of UVs, the ability of researchers to explore the deep waters has been enhanced extremely (Yu et al. 2017; Campos et al. 2017). Nowadays, UVs are turning out to be more popular, particularly for defence purposes and ecological monitoring (Londhe et al. 2017; Yang et al. 2013).

Robust tracking of AUV against various natural interruptions is the most important issue in this field (Tang 2016; Verma 2022). Here, it is essential to follow a more precise tracking desire trajectory; as a result, the energy dissipation could be eliminated (Verma and Chakraborty 2019). Moreover, it is difficult to control the movement of the AUV owing to its high time-varying, nonlinearity, uncertain nature in hydrodynamic coefficients, and the turbulences by ocean currents (Batista et al. 2009; Li, et al. 2015a, b). To handle these issues, a wide range of robust control systems were developed in the literature. The developed controller systems for tracking AUV include conventional PID controller, optimal controllers like LQR, FC and so on (Du et al. 2016; Listwan and Pieńkowski 2017). However, each controller has its advantages and disadvantages. Therefore, several researchers merged two or three diverse controllers or combined them with a new control system to enhance their performance.

In recent times, SMC (Roy and Ghoshal 2019; Liu et al. 2017; Priya and Bandyopadhyay 2017) has been widely adopted by many researchers owing to its higher robustness in opposition to disturbances/uncertainties and parameter deviations. Nevertheless, the main challenge of SMC was the "chattering effect", which leads to instability issues, need for enhancement in the steady-state performance, high energy consumption and high complexity. Hence, to overcome the above-mentioned issues, neural network-based SoSMC for autonomous underwater vehicle is designed (Cingireddy et al. 2022; Meherkandukuri 2021; Kiran 2021). The amalgamation of SMC with other controller models also reveals improved results in both practical engineering and hypothetical research. The main contributions of this proposed work are as follows:

- It introduces a novel optimized NN-based SoSMC for controlling the AUV systems in a precise manner, where optimized NN is supposed to predict positive gain.
- In an optimized NN framework, the training is performed by a novel hybridized model via tuning the optimal weights.
- Proposes Sea Lion Distance-based FireFly algorithm which hybridizes the concept of FF and SLnO models.

The paper is arranged as follows: Sect. 2 explains the reviews on traditional AUV models. Section 3 describes the illustration of the AUV system. In addition, Sect. 4 addresses the modeling of SoSMC. Optimized NN for gain prediction model: training by new SLD-FA algorithm is represented in Sect. 5. The results are discussed in Sect. 6, and the conclusion is elucidated in Sect. 7.

2 Literature review

2.1 Related works

Wadi et al. (2019) adopted an "adaptive Nussbaum-function-based controller" to track UVs. In addition, the presented model governed the adaptation so that the gains were only adapted when it was essential. Finally, the assessment was performed using varied controllers where the developed model has revealed a better performance over existing frameworks in terms of fast convergence.

Elhaki and Shojaei (2020) have introduced a "robust NN-based output-feedback tracking controller" for AUVs. The adopted model was deployed for obtaining the highest undershoots/overshoots, better tracking convergence speed and accuracy. Moreover, a high-gain observer was exploited for approximating the velocity vector, which was essential for designing the output-feedback control. Finally, an analysis was performed to validate the effectiveness of the presented model with respect to tracking errors.

Guerrero et al. (2018) have designed a nonlinear control approach to solve path tracking issues such as external disturbances and uncertainties in AUV. Initially, the AUV model was converted into a standard form via a proper selection of state parameters. This technique was dependent on the GSTA that ensured robustness to external disturbances and modelling errors. At last, an investigation was carried out that illustrated the superiority of the adopted controller.

Qiao et al. (2017) have dealt with "trajectory tracking issue of AUVs" in the existence of external disturbances and uncertainties. Here, 3 robust controllers, known as "the min–max type controller, the saturation type controller and the smooth transition type controller" were adopted for driving an AUV in a correct path. The outcomes showed that the suggested controller was superior to the conventional methods.

Hien et al. (2018) have analysed a model that depends on the real-time UML merged with EKF algorithm. Here, the analysis was carried out in stepwise. Initially, the dynamic and physical models along with the control design of AUVs were adopted. This comprehensive design was then transformed into the execution model by deploying open-source platforms that quickly simulated this controller. Finally, during simulation, the developed controller offered high performance in terms of reliability.

Kumar and Rani (2020) suggested a hybridized tracking control strategy for AUV in the existence of unstructured and structured uncertainties. Owing to these uncertainties, the entire information regarding the dynamic model was not exactly accomplished in realistic appliances. To deal with such uncertainties, the model-free control technique was effectively merged with the model-oriented control technique. In addition, RBF-NN was deployed to estimate the dynamics precisely. Thus, the suggested model attained better performance in terms of tracking error.

Bejarbaneh et al. (2020) have introduced two diverse models for the nonlinear control system of an AUV. The initial one was PID, which optimized its gains using a hybrid PSO approach. The subsequent one was a state feedback control, which deployed the LMI technique for ensuring stability using "Lyapunov stability theory". At last, the betterment of the adopted control model was validated with controllers under robustness.

Cho et al. (2020) have developed a robust controller using TDE and a back-stepping technique for tracking the AUVs. The adopted controller was modelled based on the back-stepping technique that efficiently handled matchless disturbances and offered a well-designed process to overcome the issues on matching conditions. In addition, TDE was deployed for effectively estimate the nonlinear dynamics. At the end, the proposed controller model was examined over other controllers concerning stability analysis, robust tracking and accuracy.

2.2 Review

Table 1 explains the reviews on traditional AUV systems. Initially, the Nussbaum-function-oriented controller was deployed in Wadi et al. (2019) that offers fast convergence and it also presents minimal tracking error. Nevertheless, differences in gain tuning are not analysed. NN was exploited in Elhaki and Shojaei (2020) , which presents higher gain with better accuracy; nevertheless, it is not appropriate for 6-DOF underactuated AUVs. In addition, GSTA algorithm was introduced in Guerrero et al. (2018) that offers optimal error tracking with minimized disturbances; however, it has to focus more on overshoot. Likewise, the Lyapunov function was exploited in Qiao et al. (2017), which offers enhanced tracking of UAV and offers rapid response speed. However, it has to focus more on chattering effects. Moreover, EKF method was deployed in Hien et al. (2018), which presents minimal cost and reduced static errors; however, interface among tolls should be managed in a proper way. RBF-NN was exploited in Kumar and Rani (2020) that presents high feasibility with enhanced accuracy, however, exact dynamic knowledge should be considered. PSO was suggested in Bejarbaneh et al. (2020) that offer high robustness and reduce time consumption. However, it has to focus on low convergence rate. Finally, TDE was implemented in Cho et al. (2020), which offers improved control gain and

Table 1 Review on traditional underwater vehicle systems

Author	Methods	Features	Challenges
(Wadi et al. 2019)	Nussbaum-function-based controller	Fast convergence Reduced tracking error	Differences in gain tuning are not analysed No analysis on real-time settings
(Elhaki and Shojaei 2020)	NN	High gain Improved accuracy	It is not appropriate for 6-DOF underactuated AUVs
(Guerrero et al. 2018)	GSTA algorithm	Minimize the disturbances Optimal error tracking	No observation on overshoot
(Qiao et al. 2017)	Lyapunov function	Accurate tracking of UAV Rapid response speed	More chattering effects High initial thrust force
(Hien et al. 2018)	EKF model	Minimal cost Reduced static errors	Target response is not balanced The interface among tolls should be managed in a proper way
(Kumar and Rani 2020)	RBF-NN	High feasibility Enhanced accuracy	Exact dynamic knowledge should be considered
(Bejarbaneh et al. 2020)	PSO	Offers high robustness Reduced time consumption	Low convergence rate
(Cho et al. 2020)	TDE	Offers high control gain High stability	No analysis on the applicability of controllers in actual vehicle

high stability, but, there was no analysis on the applicability of controllers in the actual vehicle.

3 Illustration of AUV system model

3.1 Heading dynamics

The actuator will "saturate" at a lower input level if the control signal provided by the feedback law is better than possible or acceptable for safety reasons. Unless the actuator saturation is explicitly accounted for in an intended nonlinear control law design, the system behaviour is unlikely to be satisfactory when the linear control law produces control signals that are so large that the actuator is always saturated. If this isn't the case, the gain matrix should be chosen to avoid producing overly large control signals for the range of states the control system might experience. Anti-windup is based on the among actuator input (controller output) and actuator output. The IMU is a type of sensor which measures angular rate and force.

Usually, the control inputs of vehicles comprise of the elevator rudder θ_e, the differential rudder θ_d, the steering rudder θ_r and trust U. Here, U is a constant and accordingly, the vehicle trajectory is handled by controlling the motion of the vehicle through rudders (Cui et al. 2016). While controlling the attitude of AUV with yaw (β) and pitch (δ) angles, the dynamic of attitudes is addressed as a "second-order system". Also, the "dynamics of roll (ϕ), pitch (δ) and yaw(β)" have the same prototype.

The vehicle's roll is ignored, and therefore a smaller pitch angle is presumed for vehicles as revealed in Fig. 1. For the nonlinearities and disturbances, the yaw kinematics and dynamics are modeled as per Eqs. (1) and (2), in which d denotes unknown disturbances,D_1 and D_2 denote unknown constraints based on hydrodynamic coefficients,

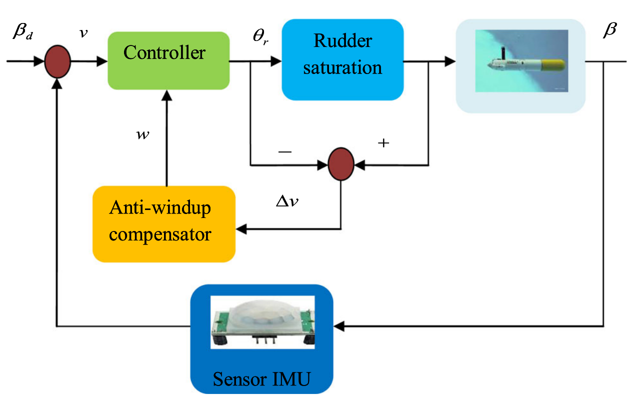

Fig. 1 Diagrammatic illustration of auxiliary system compensation model

D_3 represents control gain, and $f(u, \beta, \omega_y, t)$ denotes a nonlinear substance.

$$\dot{\beta} = \omega_y \tag{1}$$

$$\dot{\omega}_y = D_1\omega_y + D_2\psi + D_3\theta_r + f(u, \beta, \omega_y, t) + d(t) \tag{2}$$

This model is simplified and represented as shown in Eqs. (3) and (4), in which $h = [D_1.D_2]^T$,$\varphi = [\omega_y.\psi]^T$, σ symbolize the left and right slopes, and C signifies the time-varying disturbance. The major aim is to control θ_r to regulate β based on the trajectory $\beta_d(t)$ at an inestimable time period.

$$\dot{\beta} = \omega_y \tag{3}$$

$$\dot{\omega}_y = h^T\varphi + D_3\theta_r + C \tag{4}$$

The tracking error is formulated as $e = \beta(t) - \beta_d(t) \to 0,\ t \to \infty$, and its time derivative is computed as per Eq. (5).

$$\dot{e} = \dot{\beta} - \dot{\beta}_d = \omega_y - \dot{\beta}_d \tag{5}$$

Two assumptions are formulated to assist the control model.

Assumption 1 The parameter C lies in the range of $|C| \le \rho$, in which ρ represents the unidentified upper bound and $\rho > 0$. In addition, β and $\dot{\beta}$ are taken as the computable outputs.

Assumption 2 Gain D_3 is imprecise; however, its signs and upper bounds are recognized $\left(0 < D_3 < \bar{D_3}\right)$; here, $\bar{D}_3$ is a known positive constant.

3.2 Motion formulation

The dynamic form of AUV includes "inertia-referenced frame and body-referenced frame", which are exploited to demonstrate the motion of AUV (Cui et al. 2016). The AUV is positioned at the CB, and it has the "body-referenced x-axis, y-axis and z-axis. Accordingly,ϕ at x-axis is in positive counterclockwise direction, β at the y-axis is in positive turning towards left, and δ at the z-axis is positive towards bow-up direction". Further, the sideslip angle is indicated in Eq. (6), in which u_z and u_y indicate the inertial axis frames and u_x signifies the body axis frame. Likewise, the angle of attack is revealed as in Eq. (7) with regard to u_x and u_y.

$$\psi = \arctan\left(\frac{u_z}{\sqrt{u_x^2 + u_y^2}}\right) \tag{6}$$

$$\alpha = -\arctan\left(\frac{u_y}{u_x}\right) \tag{7}$$

The kinematics of AUV is demonstrated as shown in Eqs. (8) and (9), in which ω_x,ω_y and ω_z denote angular velocities in the body-referenced frame.

$$\begin{bmatrix} \dot{x} \\ \dot{y} \\ \dot{z} \end{bmatrix} = \begin{bmatrix} \cos\delta\cos\beta & \sin\beta\sin\phi - \sin\delta\cos\beta\cos\phi & \sin\beta\cos\phi + \sin\delta\cos\beta\sin\phi \\ \sin\delta & \cos\delta\cos\phi & -\cos\delta\sin\phi \\ -\cos\delta\sin\phi & \cos\beta\sin\varphi + \sin\delta\sin\beta\cos\phi & \cos\beta\cos\phi - \sin\delta\sin\beta\sin\phi \end{bmatrix} \begin{bmatrix} u_x \\ u_y \\ u_z \end{bmatrix} \tag{8}$$

$$\begin{bmatrix} \dot{\beta} \\ \dot{\delta} \\ \dot{\phi} \end{bmatrix} = \begin{bmatrix} 0 & \sec\delta\cos\phi & -\sec\delta\sin\phi \\ 0 & \sin\phi & \cos\phi \\ 1 & -\tan\delta\cos\phi & \tan\delta\sin\phi \end{bmatrix} \begin{bmatrix} \omega_x \\ \omega_y \\ \omega_z \end{bmatrix} \tag{9}$$

4 Modelling of SoSMC

4.1 SMC

The SMC (Liu et al. 2017) portrays "the modelling of a sliding mode surface, $x = 0$ to signify a lower order system when compared over the selected plant". Therefore, it is indicated as $x = e + [\lambda \times e(t)]$, in which $\lambda > 0$ is regarded as a modelling constraint.

The mathematical model of SMC law is shown in Eq. (10), in which $T_x(t)$ as well as $T_{eq}(t)$ point out the discontinuous and equivalent part of SMC. The term $T_x(t)$ is executed as per Eq. (11), where $\mu^{(1)}$ and $\mu^{(2)}$ symbolize the positive gain and the sliding surface of SMC is represented by x. Likewise, the term $T_{eq}(t)$ is attained as revealed in Eq. (12), where *wt* denotes the weighting factor.

$$v(t) = T_x(t) + T_{eq}(t) \tag{10}$$

$$T_x(t) = \mu^{(1)} \int_0^t \mathrm{sign}(x)dt + \mu^{(2)}|x|^{0.5}\mathrm{sign}(x) \tag{11}$$

$$T_{eq} = {D_3}^{-1}\left(-h^T\varphi - C + \ddot{\psi}_d - \lambda(\omega_y - \dot{\psi}_d)\right) \tag{12}$$

4.2 Proposed SoSMC model

The model of SMC includes continuous as well as discontinuous parts that represent the operating mode at lower and higher frequencies, respectively. The variations in the desired state and current state of the system are assumed to be x. The chatter effect creates instant unknown and rapid differences in controlling signal, which leads to poorer computation of FoSMC. Actually, these variations are caused owing to sign function that could be separated by SoSMC. The adopted SoSMC model is portrayed in Eq. (13).

$$v(t) = T_{eq} + T_q.\mathrm{wt} \tag{13}$$

Accordingly, the sliding surface x is formulated as shown in Eq. (14), where ($\mu^{(1)}$,$\mu^{(2)}$,φ^0,$Q(m)$,$L(m)$) denotes the gains from the positive approach,e denotes the current error, and $\dot{e}$ denotes the previous error.

$$\mu^{(1)} > \frac{\varphi^0}{Q(m)} \geq 0 \text{ and } (\mu^{(2)})^2 \geq 4\frac{\varphi^0}{(K(m))^2}\frac{\mu^{(2)}Q(m)+\varphi^0}{\mu^{(2)}L(m)+\varphi^0} > 0$$

$$x = \lambda e + \dot{e} \tag{14}$$

The objective function (Obj) of the adopted work is to minimize the current error present in the SoSMC model, which is defined in Eq. (15).

$$\mathrm{Obj} = \mathrm{Min}(e) \tag{15}$$

The optimized NN is used to predict the positive gain $\mu^{(1)}$ by giving the previous error and current error as the input.

5 Optimized NN for gain prediction model: training by New SLD-FA algorithm

5.1 Optimized neural network

In this proposed model, the NN (TC et al. 2019) optimizes the positive gain $\mu^{(1)}$. NN (Mohan et al. 2016) considers the previous error ($\dot{e}$) as well as the current error (e) (totally denoted by E) as input, which is symbolized as in Eq. (16), where nu denotes the total count of errors.

$$E = \{E_1, E_2, \ldots\ldots E_{nu}\} \tag{16}$$

The model comprises input, output, as well as hidden layers. In Eq. (17), the output of the hidden layer $q^{(H)}$ is portrayed, in which A indicates the "activation function", $\frown{i}$ and j denote the neurons of hidden as well as input layers, respectively, $W^{(H)}_{\left(B\frown{i}\right)}$ symbolizes bias weight to $\frown{i}$th hidden neuron, $n_{\frown{i}}$ signifies input neuron count, and $W^{(H)}_{\left(j\frown{i}\right)}$ signifies the weight from jth input neuron to $\frown{i}$th hidden neuron. The output $\hat{G}_o$ is represented as in Eq. (18), in which $\hat{o}$ is the output neurons, n_h points out the hidden neuron count,$W^{(G)}_{(B\hat{o})}$ denotes output bias weight to the $\hat{o}$th output layer, and the weight from $\widehat{i}$th hidden layer to $\hat{o}$th output layer is represented by $W^{(G)}_{\left(\widehat{i}\,\hat{o}\right)}$. Therefore, the error amongst the predicted and actual values is computed as per Eq. (19) which should be minimized. In Eq. (19), n_G symbolizes the output neuron count and $G_{\hat{o}}$ and $\hat{G}_{\hat{o}}$ refer to the actual and predicted output, respectively.

$$q^{(H)} = A\left(W^{(H)}_{\left(B\,\widehat{i}\right)} + \sum_{j=1}^{n_i} W^{(H)}_{\left(j\,\widehat{i}\right)} E\right) \tag{17}$$

$$\hat{G}_{\hat{o}} = A\left(W^{(G)}_{(B\hat{o})} + \sum_{\widehat{i}=1}^{n_h} W^{(G)}_{\left(\widehat{i}\,\hat{o}\right)} q^{(H)}\right) \tag{18}$$

$$Er^* = \underset{\left\{W^{(H)}_{\left(B\,\widehat{i}\right)},W^{(H)}_{\left(j\,\widehat{i}\right)},W^{(G)}_{(B\hat{o})},W^{(G)}_{\left(\widehat{i}\,\hat{o}\right)}\right\}}{\arg\min} \sum_{=1}^{n_G} \left|G_{\hat{o}} - \hat{G}_{\hat{o}}\right| \tag{19}$$

The training of the NN model is done by means of a new SLD-FA algorithm by optimizing the weights $W = W^{(H)}_{\left(B\,\widehat{i}\right)}, W^{(H)}_{\left(j\,\widehat{i}\right)}, W^{(G)}_{(B\hat{o})}$ and $W^{(G)}_{\left(\widehat{i}\,\hat{o}\right)}$.

5.2 Proposed SLD-FA algorithm

Although the conventional FF model (Fister et al. 2013) presents precise estimations, it also includes few drawbacks like "high probability of being trapped in local optima". Therefore, to overcome the drawbacks of existing FF, the concept of SLnO (Masadeh et al. 2019) is merged with it to introduce a new model. Hybrid optimization algorithms have been reported to be promising for certain search problems (Beno et al. 2014). The procedure of the adopted SLD-FA model is as follows: Fireflies are regarded as fascinating insects. The most noticeable feature of fireflies is their flashing light that involves two basic features like warning of hunters as well as attraction. Various rules govern the flashing light. As a result, the distance w gets increased when the intensity of light H is reduced.

For modelling a precise FF model, two key issues are taken into account. They are "attraction formulation and variations in H". Accordingly, H indicating the solution Y is almost equal to the fitness value. The light intensity $H(w)$ is varied based on Eq. (20), where H_0 refers to the "light intensity achieved from source, and the light absorption is computed by deploying the absorption coefficient of light denoted by γ".

$$H(w) = H_0 e^{-\gamma w^2} \tag{20}$$

Equation (21) could be used to portray attractiveness ξ, where ξ_0 points out the attraction level at $w = 0$. Also, the light intensity and ξ is approximately same.

$$\xi = \xi_0 e^{-\gamma w^2} \tag{21}$$

The proposed contribution of the adopted hybrid SLD-FA model is as follows: Conventionally, the distance $\left(w_{ij}\right)$ between two fireflies O_i and O_j is computed based on the issue of dimensionality. In this work, the distance between the fireflies is computed on the basis of the distance formulation of the SLnO algorithm, which is specified in Eq. (22). In Eq. (22), $\overrightarrow{O_{\text{rnd}}}(t)$ signifies the random sea lion, which is chosen from the current population and $\overrightarrow{B}$ denotes the random vector that lies between 0 and 1.

$$w_{ij} = \left\|O_i - O_j\right\| = \left|2\overrightarrow{B}.\overrightarrow{O_{\text{rnd}}}(t) - \overrightarrow{O}(t)\right| \tag{22}$$

Accordingly, the i^{th} firefly's movement gets attracted to a more attractive firefly j, which is formulated as per Eq. (23). In Eq. (23), ε_i symbolizes an arbitrary integer and α denotes the randomization factor

$$O_i^* = O_i + \xi_0 e^{-\gamma w_{ij}^2}\left(O_j - O_i\right) + \alpha\varepsilon_i \tag{23}$$

Algorithm 1 reveals the pseudo-code of the SLD-FA approach.

Algorithm 1: Proposed SLD-FA approach
Initialize the population of Firefly
Calculate the intensity of light
First iteration, it
While $it = it_{\max}$
For all i
For all j
Compute the distance w_{ij} on the basis of SLnO update as shown in Eq. (22)
Move firefly i towards j as per Eq. (23)
end j
end j
Compute the novel solutions
Determine the current global best
end while

6 Results and discussion

6.1 Experimental set-up

The adopted SLDFA-SoSMC based controller was implemented in "MATLAB 2020a", and the outcomes were observed. Here, the nominal model constraints like $D_1 = -4.695$, $D_2 = 10.735$, $D_3 = 1.8207$ and $h = [-4.685, 10.735]^T$ were considered to reveal the performance of SoSMC in AUV system. In addition, the preliminary states of the AUV system were fixed as $\omega_y(0) = 3^\circ/s$ and $\beta(0) = 10^\circ$. Likewise the preliminary states of the estimated constraints were chosen as $\hat{C}(0) = 0.6, \hat{\mu}(0) = 0, \hat{h}(0) = [-1, 2]^T$, $\hat{\omega}_y(0) = 0$ and $\hat{D}_3(0) = 0$. Moreover, the disturbance caused based on outer source was selected as $C = \sin(0.01t)0.55 + \sin(0.1t)0.33 + \cos(0.02t)0.25 \quad + 0.3\cos(0.2t).\sin(0.1t)$.

At last, the nonlinear saturation of AUV was denoted by δ_r, which was set as 12°.The superiority of the proposed model has been compared to optimization algorithms, namely GW-SMC (Mirjalili et al. 2014), FF-SoSMC (Fister et al. 2013), SLnO-SoSMC (Masadeh et al. 2019), POA-SoSMC (Goel 2014), GW-SoSMC (Roy and Ghoshal 2019), GSTA (Guerrero et al. 2018) and Hybrid PSO (Bejarbaneh et al. 2020). Here, the analysis was done with respect to steady-state response and absolute error.

6.2 Steady-state response

Table 2 demonstrates the steady-state response (in sec) of the adopted model over traditional models. Here the results are accomplished for four set points, namely, "set point 1, set point 2, set point 3 and set point 4". On seeing the results, the proposed SLDFA-SoSMC model has attained improved rise time and settling time when compared to the traditional models for all set points. In addition, the overshoot accomplished by the SLDFA-SoSMC model is much lower when compared to the other traditional models. The enhanced steady-state response thus guarantees the improved performance of the presented model. The settling time of the presented SLDFA-SoSMC model for set point 1 is 28.52% and 8.48% better than GW-SMC and GW-SoSMC models. On analysing set point 1, the overshoot of the presented SLDFA-SoSMC model has attained lower rise time as well as settling time, whereas the peak time of the presented and existing models are found to be similar.

On examining the results attained for set point 3, the proposed model has exposed a minimal steady-state response with the conventional models. On analysing the set point 4, the overshoot of the presented SLDFA-SoSMC model is 3.61%, 14.11%, 0.01%, 14.10%, 1.52%, 3.61% and 14.11% superior to GW-SMC, FF-SoSMC, SLnO-SoSMC, POA-SoSMC, GW-SoSMC, GSTA and Hybrid PSO. Altogether, the steady-state response of the adopted SLDFA-SoSMC model had been verified over other existing models.

6.3 Error analysis

Figure 2 exhibits the error analysis of the proposed (SLDFA-SoSMC) scheme with the existing scheme for a varied time interval that ranges from 0 to 200 s. From the graph, the error attained by the presented work is lower than the existing models, ensuring that the deviation between the predicted and desired yaw angle is minimal. From Fig. 2, the error attained by the presented work at 150th sec is 0.001, which is 99.99%, 99.98%, 99.98%,

Table 2 Steady-state response: Adopted work over existing works for varied set points

Methods	Rise Time (sec)	Settling Time (sec)	Settling Minimum	Settling Maximum	Overshoot	Undershoot	Peak position	Peak Time (sec)
Set point 1								
GW-SMC (Mirjalili et al. 2014)	0	5.460	25.138	33.863	22.441	0	33.863	2
FF-SoSMC (Fister et al. 2013)	0.141	8.146	26.966	37.871	26.578	0	37.871	2
SLnO-SoSMC (Masadeh et al. 2019)	0.141	8.146	26.967	37.87	26.577	0	37.87	2
POA-SoSMC (Goel 2014)	0.141	8.146	26.966	37.87	26.577	0	37.87	2
GW-SoSMC (Roy and Ghoshal 2019)	0.142	8.146	27.13	37.931	26.691	0	37.931	2
GSTA (Guerrero et al. 2018)	0	5.460	25.138	33.863	22.441	0	33.863	2
Hybrid PSO (Bejarbaneh et al. 2020)	0.141	8.146	26.966	37.871	26.578	0	37.871	2
SLDFA-SoSMC	0.141	8.145	26.966	37.87	26.576	0	37.87	2
Set point 2								
GW-SMC (Mirjalili et al. 2014)	0	49.901	4.2805	25.138	60.297	z0	25.138	1
FF-SoSMC (Fister et al. 2013)	0	49.538	− 3.9027	25.138	121.02	34.313	25.138	1
SLnO-SoSMC (Masadeh et al. 2019)	0	49.534	− 3.9044	25.138	120.96	34.32	25.138	1
POA-SoSMC (Goel 2014)	0	49.541	− 3.8991	25.138	121.03	34.284	25.138	1
GW-SoSMC (Roy and Ghoshal 2019)	0	49.806	− 3.8431	25.138	110.8	32.227	25.138	1
GSTA (Guerrero et al. 2018)	0	49.901	4.2805	25.138	60.297	0	25.138	1
Hybrid PSO (Bejarbaneh et al. 2020)	0	49.538	− 3.9027	25.138	121.02	34.313	25.138	1
SLDFA-SoSMC	0	49.537	− 3.9021	25.138	120.95	34.298	25.138	1
Set point 3								
GW-SMC (Mirjalili et al. 2014)	0.234	26.271	30.161	40.372	26.573	0	40.372	2
FF-SoSMC (Fister et al. 2013)	0.367	8.0414	37.021	55.042	37.148	0	55.042	2
SLnO-SoSMC (Masadeh et al. 2019)	0.367	8.0417	37.023	55.039	37.14	0	55.039	2
POA-SoSMC (Goel 2014)	0.367	8.0416	37.022	55.04	37.144	0	55.04	2
GW-SoSMC (Roy and Ghoshal 2019)	0.364	8.1365	36.712	54.806	37.216	0	54.806	2
GSTA (Guerrero et al. 2018)	0.234	26.271	30.161	40.372	26.573	0	40.372	2
Hybrid PSO (Bejarbaneh et al. 2020)	0.367	8.0414	37.021	55.042	37.148	0	55.042	2
SLDFA-SoSMC	0.367	8.0408	37.023	55.039	37.141	0	55.039	2
Set point 4								
GW-SMC (Mirjalili et al. 2014)	0	47.242	13.685	27.298	27.467	0	27.298	4
FF-SoSMC (Fister et al. 2013)	0	42.095	11.896	25.301	37.336	0	25.301	4
SLnO-SoSMC (Masadeh et al. 2019)	0	49.005	11.895	25.301	37.355	0	25.301	4

Table 2 (continued)

Methods	Rise Time (sec)	Settling Time (sec)	Settling Minimum	Settling Maximum	Overshoot	Undershoot	Peak position	Peak Time (sec)
POA-SoSMC (Goel 2014)	0	42.102	11.891	25.301	37.346	0	25.301	4
GW-SoSMC (Roy and Ghoshal 2019)	0	48.266	13.522	25.301	35.376	0	25.301	4
GSTA (Guerrero et al. 2018)	0	47.242	13.685	27.298	27.467	0	27.298	4
Hybrid PSO (Bejarbaneh et al. 2020)	0	42.095	11.896	25.301	37.336	0	25.301	4
SLDFA-SoSMC	0	49.012	11.895	25.301	37.374	0	25.301	4

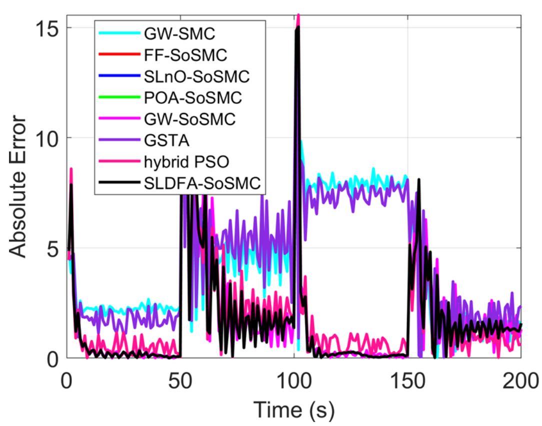

Fig. 2 Error analysis of the proposed model over the existing model for varied time in seconds

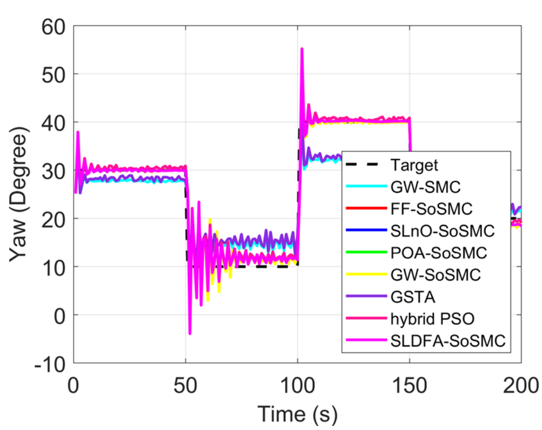

Fig. 3 Yaw angle analysis of adopted scheme over the existing schemes for varied time in seconds

99.98%, 99.98%, 99.98% and 99.98% superior to existing approaches like "GW-SMC, FF-SoSMC, SLnO-SoSMC, POA-SoSMC and GW-SoSMC", respectively. The error value accomplished by proposed model at 70th sec is 99.98%, 99.97%, 99.97%, 99.97%, 99.97%, 99.97% and

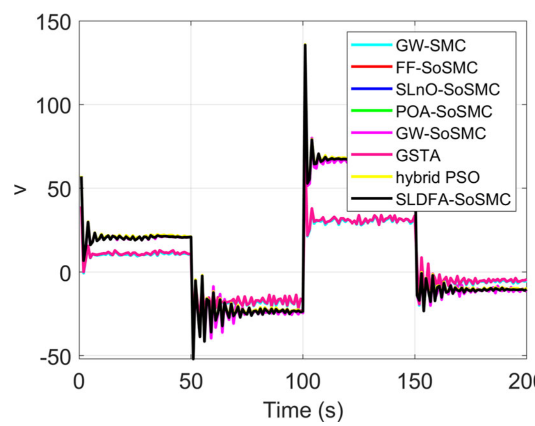

Fig. 4 Controller Response of adopted scheme over the existing schemes concerning varied time in seconds

99.97% superior to existing approaches like "GW-SMC, FF-SoSMC, SLnO-SoSMC, POA-SoSMC and GW-SoSMC", respectively. Therefore the adopted SLDFA-SoSMC model reveals a superior performance with error minimization.

6.4 Yaw angle analysis

The yaw angle control analysis for the presented SLDFA-SoSMC over the existing methods is described in this section. On observing Fig. 3, the deviation found between the target and predicted results with the presented method is negligible, whereas the existing methods have revealed a higher deviation. More specifically, from Fig. 3, the proposed work at 70th sec is 9.09% deviated from the actual target, whereas the existing scheme like "GW-SMC, FF-SoSMC, SLnO-SoSMC, POA-SoSMC and GW-SoSMC" exhibits a deviation of 33.33% from the target. Likewise, when the time interval is at 10 s, the adopted model is almost similar to the target value, whereas the conventional methods show a deviation of 6.67% from the target. Thus

Table 3 RMSE analysis for the adopted scheme over the existing schemes for different set points

Methods	Set point 1	Set point 2	Set point 3	Set point 4
GW-SMC (Mirjalili et al. 2014)	2.4339	5.5542	8.0705	2.5787
FF-SoSMC (Fister et al. 2013)	1.4376	4.8466	3.0718	2.4868
SLnO-SoSMC (Masadeh et al. 2019)	1.4375	4.8468	3.0716	2.4867
POA-SoSMC (Goel 2014)	1.4375	4.8477	3.0716	2.4877
GW-SoSMC (Roy and Ghoshal 2019)	1.4433	4.9897	3.0752	2.5785
GSTA (Guerrero et al. 2018)	2.0728	5.9458	7.6288	2.9218
Hybrid PSO (Bejarbaneh et al. 2020)	1.5719	5.0203	3.1699	2.3349
SLDFA-SoSMC	1.4374	4.8462	3.0715	2.4859

Table 4 MAPE analysis for the adopted scheme over the existing schemes for different set points

Methods	Set point 1	Set point 2	Set point 3	Set point 4
GW-SMC (Mirjalili et al. 2014)	7.8667	50.622	19.813	9.8518
FF-SoSMC (Fister et al. 2013)	1.824	32.836	2.2903	9.6795
SLnO-SoSMC (Masadeh et al. 2019)	1.8239	32.83	2.2902	9.6799
POA-SoSMC (Goel 2014)	1.824	32.848	2.2901	9.6829
GW-SoSMC (Roy and Ghoshal 2019)	1.8413	34.217	2.431	10.155
GSTA (Guerrero et al. 2018)	6.4062	55.003	18.717	11.976
Hybrid PSO (Bejarbaneh et al. 2020)	2.7155	36.403	3.3498	8.0674
SLDFA-SoSMC	1.8236	32.832	2.2899	9.6779

the enhanced performance of the proposed work is revealed effectively with lesser deviation from the target.

6.5 Controller response

Figure 4 illustrates the analysis of controller response v at varied time intervals that ranges from 0 to 200 s. On observing the graph, it is noticed that the control signal for the presented work has reached the target value with minimal deviation. In contrast, the control signals of the compared traditional models such as “GW-SMC, FF-SoSMC, SLnO-SoSMC, POA-SoSMC and GW-SoSMC” reveal a higher deviation from the target. Thus the better controlling response of the proposed SLDFA-SoSMC model has been validated efficiently.

6.6 RMSE analysis

The RMSE analysis, and the MAPE analysis of the proposed SLDFA-SoSMC model over traditional models for varied set points, are exposed in Tables 3 and 4 in that order. On observing the attained outcomes, the implemented model has obtained minimal error values for all set points when compared to other methods. More specifically, from Table 3, the RMSE values attained by the adopted scheme for set point 1 is found to be minimal, which is 40.94%, 1.39%, 0.69%, 0.69% and 0.41% better than traditional models such as “GW-SMC, FF-SoSMC, SLnO-SoSMC, POA-SoSMC and GW-SoSMC”, respectively. In addition, the RMSE values accomplished by the implemented scheme for set point 3 is 3.0715, which is 61.94%, 0.97%, 0.33%, 0.33% and 0.12% superior to existing models such as “GW-SMC, FF-SoSMC, SLnO-SoSMC,

Table 5 Analysis on Euclidean Distance: presented model with Traditional models for varied set points

Methods	Set point 1	Set point 2	Set point 3	Set point 4
GW-SMC (Mirjalili et al. 2014)	17.21	39.274	57.067	18.234
FF-SoSMC (Fister et al. 2013)	10.165	34.271	21.721	17.584
SLnO-SoSMC (Masadeh et al. 2019)	10.165	34.272	21.719	17.583
POA-SoSMC (Goel 2014)	10.165	34.278	21.72	17.591
GW-SoSMC (Roy and Ghoshal 2019)	10.206	35.282	21.745	18.233
GSTA (Guerrero et al. 2018)	14.657	42.043	53.944	20.66
Hybrid PSO (Bejarbaneh et al. 2020)	11.115	35.499	22.415	16.51
SLDFA-SoSMC	10.164	34.268	21.719	17.578

Table 6 Computing time of proposed over traditional methods

Methods	Time (s)
GW-SMC	1316.2
FF-SoSMC	1330.3
SLnO-SoSMC	1435.3
POA-SoSMC	1420.4
GW-SoSMC	1443.2
GSTA	1476.6
Hybrid PSO	1486.2
SLDFA-SoSMC	1025.9

POA-SoSMC and GW-SoSMC", respectively. Also, from Table 4, the MAPE of the adopted model at set point 4 has accomplished a minimal value of 9.6779, which is 1.79%, 1.65%, 5.17% and 4.93% superior to existing models such as GW-SMC, FF-SoSMC, POA-SoSMC and GW-SoSMC. As a result, the improved performance of the adopted model is validated using RMSE analysis.

6.7 Analysis on Euclidean distance

The analysis on Euclidean distance accomplished by the presented model over traditional models is represented in Table 5. On analyzing the outcomes, the Euclidean distance achieved by the adopted model is minimal when compared to the traditional models. Particularly, the adopted scheme for set point 1 is found to be minimal which is 40.94%, 0.69%, 0.69%, 0.69% and 0.41% better than traditional models like "GW-SMC, FF-SoSMC, SLnO-SoSMC, POA-SoSMC and GW-SoSMC", respectively. Thus, the analysis on Euclidean distance proves the betterment of implemented SLDFA-SoSMC over other models.

6.8 Computing time

This section discusses the proposed method's computing time compared to other existing methods. The results obtained for the proposed SLDFA-SoSMC with the traditional methods is depicted in Table 6. From the table, it can be noticed that the proposed model consumes less time when compared with other traditional models. The adopted method is 22.05%, 22.88%, 28.52%, 27.77%, 28.91%, 43.93% and 44.86% better than the traditional methods like "GW-SMC, FF-SoSMC, SLnO-SoSMC, POA-SoSMC, GW-SoSMC, GSTA and Hybrid PSO", respectively.

6.9 Practical implication

Neural networks have a distinctive ability to extract meaning from inaccurate or composite data to determine patterns and detect trends too complicated for the other computer techniques and the human brain. Also, NN are proved to be energy efficient in the literature (Park and Sung 2016; Roukhami et al. 2019; Tu et al. 2019; Tang et al. 2020). In particular, Park and Sung (2016) have introduced an FPGA-based fixed-point DNN system using on-chip memory, which results in very less power consumption of 5 Watt at the full speed operation. Besides, Roukhami et al. (2019) have employed very less energy-consuming NN FPGA accelerators to identify Tag-less Remote individuals by means of Capacitive Sensors. The experimental result shows that the developed system consumes less energy of 39 nJ. Likewise, (Tu et al. 2019) have implemented an energy-efficient NN on heterogeneous FPGA and GPU devices, resulting in low energy consumption. In addition, (Tang et al. 2020) have proven the energy efficiency (4.73 GOPS/W) by presenting high energy efficiency model using CNN on FPGA. Moreover, lightweight neural networks are there that achieves high-speed manipulation with low energy is consumption. Hence, NN is considered more feasible to be used in UAV scenarios.

7 Conclusion

This paper had introduced a novel NN-based SoSMC for control of yaw angle in a precise manner. A precise analysis was done to validate the improvement of the proposed model with the conventional models under various measures. The RMSE values attained by the adopted scheme for set point 1 was 40.94%, 1.39%, 0.69%, 0.69% and 0.41% better than traditional models like 'GW-SMC, FF-SoSMC, SLnO-SoSMC, POA-SoSMC and GW-SoSMC", respectively. Besides, the RMSE values accomplished by the implemented scheme for set point 3 was 3.0715, which was 61.94%, 0.97%, 0.33%, 0.33% and 0.12% superior to traditional models like "GW-SMC, FF-SoSMC, SLnO-SoSMC, POA-SoSMC and GW-SoSMC", respectively. Hence, the supremacy of the proposed SLDFA-SoSMC scheme has been demonstrated effectively. The better performance of the proposed model is due to the deployment of a novel optimized NN-based SoSMC, which precisely controls the AUV systems, with the optimized NN predicting positive gain. A novel SLDFA-SoSMC algorithm performs the training in an optimized NN framework by tuning the optimal weights. The future direction of this work can be concentrated on real-time implementation.

Funding The authors have not disclosed any funding.

Data availability No new data were generated or analysed in support of this research.

Declarations

Conflict of interest No potential conflict of interest was reported by the author.

Ethical approval This paper does not contain any studies with human participants or animals performed by any of the authors.

Human or animals rights participants This article does not contain any studies with human participants performed by any of the authors.

Informed consent Informed consent was obtained from all individual participants included in the study.

References

Batista P, Silvestre C, Oliveira P (2009) A sensor-based controller for homing of underactuated AUVs. IEEE Trans Rob 25(3):701–716

Bejarbaneh EY, Masoumnezhad M, Armaghani DJ, Pham BT (2020) Design of robust control based on linear matrix inequality and a novel hybrid PSO search technique for autonomous underwater vehicle. Appl Ocean Res. https://doi.org/10.1016/j.apor.2020.102231

Beno MM, Valarmathi IR, Swamy SM, Rajakumar BR (2014) Threshold prediction for segmenting tumour from brain MRI scans. Int J Imaging Syst Technol 24(2):129–137

Campos E, Chemori A, Creuze V, Torres J, Lozano R (2017) Saturation based nonlinear depth and yaw control of underwater vehicles with stability analysis and real-time experiments. Mechatronics 45:49–59

Cho GR, Li J-H, Park D, Jung JH (2020) Robust trajectory tracking of autonomous underwater vehicles using back-stepping control and time delay estimation. Ocean Eng. https://doi.org/10.1016/j.oceaneng.2020.107131

Cingireddy AR, Ghosh R, Melapu VK, Joginipelli S, Kwembe TA (2022) Classification of parkinson's disease using motor and non-motor biomarkers through machine learning techniques. Int J Quant Struct Prop Relat (IJQSPR) 7(2):1–21

Cui R, Zhang X, Cui D (2016) Adaptive sliding-mode attitude control for autonomous underwater vehicles with input nonlinearities. Ocean Eng 123:45–54

Du H, Yu X, Chen MZQ, Li S (2016) Chattering-free discrete-time sliding mode control. Automatica 68:87–91

Elhaki O, Shojaei K (2020) A robust neural network approximation-based prescribed performance output-feedback controller for autonomous underwater vehicles with actuators saturation. Eng Appl Artif Intell 88:103382

Fister I, Fister I, Yang X-S, Brest J (2013) A comprehensive review of firefly algorithms. Swarm Evol Comput 13:34–46

Goel S (2014) Pigeon optimization algorithm: a novel approach for solving optimization problems, In: Proceedings of the international conference on data mining and intelligent computing (ICDMIC), New Delhi, pp 1–5

Guerrero J, Antonio E, Manzanilla A, Torres J, Lozano R (2018) Autonomous underwater vehicle robust path tracking: auto-adjustable gain high order sliding mode controller. IFAC-PapersOnLine 51(13):161–166

Hien NV, He NV, Diem PG (2018) A model-driven implementation to realize controllers for autonomous underwater vehicles. Appl Ocean Res 78:307–319

Kiran BK (2021) Indian music classification using neural network based dragon fly algorithm. J Comput Mech Power Syst Control 4(3):32–40

Kumar N, Rani M (2020) An efficient hybrid approach for trajectory tracking control of autonomous underwater vehicles. Appl Ocean Res 95:102053. https://doi.org/10.1016/j.apor.2020.102053

Li B, Su T-C (2016) Nonlinear heading control of an autonomous underwater vehicle with internal actuators. Ocean Eng 125:103–112

Li D-j, Chen Y-h, Shi J-G, Yang C-J (2015a) Autonomous underwater vehicle docking system for cabled ocean observatory network. Ocean Eng 109:127–134

Li S, Wang X, Zhang L (2015b) Finite-time output feedback tracking control for autonomous underwater vehicles. IEEE J Oceanic Eng 40(3):727–751

Listwan J, Pieńkowski K (2017) Control of five-phase induction motor with application of second-order sliding-mode Direct Field-Oriented method, In: Proceedings of the IEEE conference publications, pp 1–6

Liu L, Mei K, Ding S (2017) Controller design of second order sliding mode control systems with mismatached perturbations, In: Proceedings of the IEEE conference publications, pp 752–757

Londhe PS, Mohan S, Patre BM, Waghmare LM (2017) Robust task-space control of an autonomous underwater vehicle-manipulator system by PID-like fuzzy control scheme with disturbance estimator. Ocean Eng 139:1–13

Mahdi H, Al-Bander B, Alwan MH, Abood MS, Hamdi MM (2021) Vehicular networks performance evaluation based on downlink scheduling algorithms for high-speed long term evolution–vehicle. Int J Interact Mobile Technol 15(21):52–56

Masadeh R, Mahafzah B, Sharieh A (2019) Sea lion optimization algorithm. Int J Adv Comput Sci Appl 10:388–395

Mastan Sharif SK, Satya Prasad K, Venkata Rao D (2018) Adaptive decision feedback equalizer with dynamic principle for echo cancellation. Trans Inst Meas Control 40(16):4455–4471

Meherkandukuri (2021) Deep convolutional neural network for emotion recognition via EEG Signal. J Comput Mech Power Syst Control 4(2):18–24

Mirjalili S, Mirjalili SM, Lewis A (2014) Grey wolf optimizer. Adv Eng Softw 69:46–61

Mohan Y, Chee SS, Xin DKP, Foong LP (2016) Artificial neural network for classification of depressive and normal in EEG. In: Proceedings of the IEEE EMBS conference on biomedical engineering and sciences (IECBES)

Park J, Sung W (2016) FPGA based implementation of deep neural networks using on-chip memory only. In: Proceedings of the 2016 IEEE international conference on acoustics, speech and signal processing (ICASSP), pp 1011–1015. IEEE

Petrich J, Stilwell DJ (2011) Robust control for an autonomous underwater vehicle that suppresses pitch and yaw coupling. Ocean Eng 38(1):197–204

Priya PSL, Bandyopadhyay B (2017) Discrete time sliding mode control for uncertain Delta operator systems with infrequent output measurements. Eur J Control 33:52–59

Qianwen Z (2021) Integrating renewable energy sources in electric vehicles via optimization assisted model. J Comput Mech Power Syst Control 4(1)

Qiao L, Yi B, Wu D, Zhang W (2017) Design of three exponentially convergent robust controllers for the trajectory tracking of autonomous underwater vehicles. Ocean Eng 134:157–172

Roukhami M, Lazarescu MT, Gregoretti F, Lahbib Y, Mami A (2019) Very low power neural network FPGA accelerators for tag-less remote person identification using capacitive sensors. IEEE Access 7:102217–102231

Roy RG, Ghoshal D (2019) A novel adaptive second-order sliding mode controller for autonomous underwater vehicles. Adapt Behav 29(1):39–54

Shaik MS, Prasad KS, Shaik RA, Rao DV (2016) Acoustic echo cancellation using computationally efficient adaptive algorithm techniques. Aptikom J Comput Sci Inf Technol 1(2):57–62

Sinjari B, D'Addazio G, Traini T, Varvara G, Scarano A, Murmura G, Caputi SA (2019) 10-year retrospective comparative human study on screw-retained versus cemented dental implant abutments. J Biol Regul Homeost Agents 33:787–797

Tang Y (2016) Vehicle tracking and counting based on vehicle recognition". China Comput Commun J 13:97–98

Tang Y, Dai R, Xie Y (2020) Optimization of energy efficiency for fpga-based convolutional neural networks accelerator. J Phys Conf Ser 1487(1):012028

Tc SR, Ss TR, Subrahmanyam JBV (2019) Enhanced deep convolutional neural network for fault signal recognition in the power distribution system. J Comput Mech Power Syst Control 2:39–46

Tu Y, Sadiq S, Tao Y, Shyu ML, Chen SC (2019) A power efficient neural network implementation on heterogeneous fpga and gpu devices. In: 2019 IEEE 20th international conference on information reuse and integration for data science (IRI): pp 193–199. IEEE

Verma G (2022) Secure VM migration in cloud: multi-criteria perspective with improved optimization model. Wireless Pers Commun 124(1):75–102. https://doi.org/10.1007/s11277-021-09319-w

Verma G, Chakraborty R (2019) A hybrid privacy preserving scheme using finger print detection in cloud environment. Ing Des Syst d Inf 24(3):343–351

Wadi A, Mukhopadhyay S, Lee J-H (2019) A novel disturbance-robust adaptive trajectory tracking controller for a class of underactuated autonomous underwater vehicles. Ocean Eng 189:106377

Woods SA, Bauer RJ, Seto ML (2012) Automated ballast tank control system for autonomous underwater vehicles. IEEE J Oceanic Eng 37(4):727–739

Yang H, Wang C, Zhang F (2013) Brief paper: a decoupled controller design approach for formation control of autonomous underwater vehicles with time delays. IET Control Theory Appl 7(15):1950–1958

Yu C, Xiang X, Lapierre L, Zhang Q (2017) Nonlinear guidance and fuzzy control for three-dimensional path following of an underactuated autonomous underwater vehicle. Ocean Eng 146:457–467